Chemical Equilibrium Laminar or Turbulent Three-Dimensional Viscous Shock-Layer Flows

R.R. Thareja,* K.Y. Szema,† and C.H. Lewis‡
Virginia Polytechnic Institute and State University, Blacksburg, Virginia

A computational method has been developed to predict three-dimensional hypersonic laminar or turbulent shock-layer flows for perfect gas or equilibrium air. A two-layer eddy-viscosity model is used for the turbulent regime. The thermodynamic and transport properties for air are obtained by interpolation within a two-dimensional table or from curve-fit data. Comparisons are made for air in chemical equilibrium and perfect gas for laminar and turbulent flow over a 7-deg half-angle spherically blunted cone at various flight altitudes with a cold, moderately cool, and an adiabatic wall for angles of attack up to 20 deg. Surface pressure and wall heat-transfer distributions, force and moment coefficients, and execution times are compared for some sample cases. This method can be used to predict viscous flowfields in chemical equilibrium over axisymmetric re-entry vehicles at angles of attack up to 25 deg.

Nomenclature

C_{f_s} = skin-friction coefficient in the streamwise direction
C_{f_ϕ} = skin-friction coefficient in the transverse direction
C_p = constant pressure specific heat
h = static enthalpy $= h^*/U_\infty^2$
H = total enthalpy $= h + (u^2+v^2+w^2)/2$
k_t = eddy thermal conductivity $= -\overline{(\rho v)'h'}/(\epsilon^2 \partial h/\partial \eta)$
M = Mach number
n_{sh} = shock-standoff distance $= n_{sh}^*/R^*$
p = pressure $= p^*/\rho_\infty U_\infty^2$
PG = perfect gas
Pr = Prandtl number
Pr_t = turbulent Prandtl number $= C_p \mu_t / k_t$
Q_w = convective heating rate, W/m^2
r = distance from and normal to the body axis $= r^*/R^*$
R = gas constant
R^* = body nose radius
s = general surface-normal streamwise coordinate $= s^*/R^*$
T = temperature
TLU = table look-up
T^* = reference temperature $= U_\infty^2/C_p^*$
u,v,w = streamwise, normal, and cross-flow velocity components, respectively, nondimensionalized by the freestream velocity U_∞^*
W = dependent variable
Z_{cp}/L = percent length center-of-pressure location from nose
α = angle of attack
γ = ratio of specific heat
ϵ = Reynolds number parameter, $\epsilon^2 = \mu_{ref}^*/\rho_\infty U_\infty R^*$
ϵ^+ = μ_t/μ
η,ϕ = general surface-normal coordinates in the normal and cross-flow directions, respectively
θ_c = body angle in the streamwise direction
μ = viscosity $= \mu^*/\mu_{ref}^*$
μ_{ref}^* = reference viscosity $= \mu^*(T_{ref})$
μ_t = eddy viscosity $= -\overline{(\rho v)'u'}/(\epsilon^2 \partial u/\partial n)$
ρ = density $= \rho^*/\rho_\infty$

Subscripts and Superscripts

A = axial
B = Bade
C = Cohen
INV = inviscid
N = normal
P = pressure
s = streamwise
SF = skin friction
sh = conditions behind the bow shock wave
t = turbulent quantity
TOT = total
w = wall condition
∞ = dimensional freestream conditions
ϕ = transverse
0 = stagnation condition
$(^*)$ = dimensional quantity
$(\,)'$ = fluctuating value

Presented as Paper 82-0305 at the AIAA 20th Aerospace Sciences Meeting, Orlando, Fla., Jan. 11-14, 1982; submitted Jan. 22, 1982; revision received March 11, 1983.

*Graduate Student, Aerospace and Ocean Engineering Department. Student Member AIAA.

†Research Associate, Aerospace and Ocean Engineering Department. Member AIAA.

‡Professor, Aerospace and Ocean Engineering Department. Associate Fellow AIAA.

Introduction

THERE is renewed interest in the problem of computing hypersonic flow past a blunt body under flight conditions. A perfect gas model cannot accurately predict the thermodynamic and transport properties required for inviscid and viscous flowfield analyses of ballistic and lifting re-entry vehicles. Earlier investigators used a table look-up procedure[1] or curve-fit data[2] to model the thermodynamic and transport properties of air in chemical equilibrium for viscous boundary-layer flows.

Re-entry vehicles operate through a wide range of flow conditions. The complex flowfield is bounded by the body and the bow shock. Cross-flow separation may be present, and viscous effects may predominate over the entire flowfield. The full Navier-Stokes equations are elliptic in all three space dimensions, and a numerical solution is difficult and requires large computing times and storage. For moderately high values of Reynolds number, there is no need to solve the full Navier-Stokes equations.[3] The classical approach of dividing

the flowfield into a viscous boundary-layer region and an outer inviscid region becomes inaccurate for re-entry flowfields due to the presence of viscous effects throughout the entire flowfield. The parabolized Navier-Stokes (PNS) approach uses a parabolic approximation in the streamwise direction. This involves large matrix solutions, and the computing times are still quite large. The viscous shock-layer (VSL) approach developed by Murray and Lewis[4] for three-dimensional flows is parabolic in both the streamwise and cross-flow directions. Since the cross-flow momentum equation is parabolic, the cross-flow separated region on the leeward side cannot be treated. The solution for the windward region up to cross-flow separation is accurate, and the computing times are relatively small. In the viscous shock-layer solution, the entire flowfield from the body to the shock is treated with a uniform set of equations. The problems associated with the displacement-thickness interaction and edge conditions are eliminated, with vorticity interaction present in the inviscid plus boundary-layer approach. As a result, the viscous shock-layer method treats all higher-order boundary-layer effects (displacement, vorticity interaction, and longitudinal and transverse curvature, including proper matching conditions) in a straightforward and consistent manner, making the viscous shock-layer approach especially attractive for design studies.

Recently, a numerical method was developed by Szema and Lewis[5] to predict laminar, transitional and/or turbulent hypersonic flows of a perfect gas over a blunt body at angle of attack. In that approach a two-layer eddy-viscosity model proposed by Cebeci,[6] and the transition model developed by Dhawan and Narasimha[7] were used. This method has been extended to include the effect of chemically reacting air in equilibrium. Results from a table look-up procedure and curve-fit methods have been compared with those from a perfect gas analysis. The table look-up procedure, described later, is known to model the thermodynamic properties of air quite accurately, while the transport properties are curve-fits of Hansen's[8] data.

Numerical solutions were obtained for a 7-deg half-angle spherically blunted cone at a flight velocity of 6096 m/s at altitudes of 12,192, 24,384, and 48,768 m with a cold (300 K), moderately cool (2000 K), and an adiabatic wall for angles of attack up to 20 deg. Wall heat-transfer, wall pressure, force and moment coefficients, center-of-pressure locations, and execution times are compared for perfect gas and air in chemical equilibrium for some sample cases.

Analysis

The basic, three-dimensional, viscous shock-layer equations are derived from the steady Navier-Stokes equations in a surface-oriented coordinate system (s,η,ϕ). The governing equations for turbulent flow are developed using methods analogous to those presented in Refs. 9 and 10. The normal velocity v and normal coordinate η are assumed to be of order ϵ, and second-order terms are retained in the s-momentum, ϕ-momentum, and energy equations. The nondimensional turbulent-conservative form of the equations in a body-oriented coordinate system is given by Szema and Lewis.[5]

Equation of State

For a perfect gas, the equation $\rho=\rho(p,h)$ has the analytical form

$$\rho=\gamma p/[(\gamma-1)T]$$

For a gas in chemical equilibrium, the functional relation may be given by a table or an approximating analytical expression (curve-fit) as discussed in the section on thermodynamic and transport properties. The same equations are valid for laminar flow if the turbulent eddy-viscosity ϵ^+ is set to zero.

Boundary Conditions

Appropriate boundary conditions at the body surface and the shock must be specified. At the body surface or wall, no-slip and no-temperature jump conditions are used. Thus, at the wall, $u=v=w=0$, and the wall temperature or heat-transfer rate is specified. The conditions immediately behind the shock are obtained from the Rankine-Hugoniot relations.

Eddy-Viscosity Model

For turbulent flow a two-layer eddy-viscosity model introduced by Cebeci[6] consisting of an inner law based upon Prandtl's mixing-length concept and the Klebanoff[11]-Clauser[12] expression for the outer law is used. Further details on the eddy-viscosity model are given by Szema and Lewis in Ref. 5.

Thermodynamic and Transport Properties

For a perfect gas, the thermodynamic properties for specific heat and enthalpy can be expressed as

$$C_p=\gamma R/(\gamma-1) \qquad h=C_pT$$

The Prandtl number is assumed constant everywhere. The viscosity is calculated from Sutherland's viscosity[13] law:

$$\mu=1.09\text{E}-6T^{3/2}/(T+110.33)\ \text{kg/m-s}$$

For air in chemical equilibrium, a table look-up procedure or curve-fit data are used to provide the thermodynamic and transport properties as a function of the pressure and enthalpy.

Table Look-Up

A two-dimensional table was generated for the properties using the method developed by Miner et al.[1] For a given pressure and temperature, the enthalpy and density are determined using the reservoir calculations of Lordi et al.[14] The viscosity is obtained by curve-fits from the Wilke semiempirical formula,[1] while the Prandtl number is obtained by interpolation of the Hansen data.[8]

Cohen Curve-Fits

Curve-fit data are based on Cohen's fit[2] of Hansen's tables[8] for the transport properties and the Moeckel-Weston tables[15] for the thermodynamic properties of equilibrium air.

Density

The enthalpy dependence of the density is given by the curve-fit:

$$\rho_E/\rho=1.0-1.0477[1.0-(h/h_C)^{0.6123}]$$

This fit is reasonably good for the enthalpy range $0.0152\le h/h_C\le 2.0$. The maximum deviation in this range is about 25% at low enthalpy, and the average deviation for all data is about 6%.

The pressure dependence is given by the following:

$$\rho_E/\rho_C=0.0294(p/p_C)^{0.965}$$

This fit has a deviation of less than ½% over the range of pressures $10^{-4}\le p/p_C\le 10$.

Viscosity

The enthalpy dependence for the viscosity-density product is given by the curve-fit:

$$\rho_E\mu_E/\rho\mu=1.0-1.0213[1.0-(h/h_C)^{0.3329}]$$

This fit has better agreement than that for the density. The maximum deviation over the enthalpy range 0.0152

$\leq h/h_C \leq 2.0$ is about 8%, and the average deviation is about 3%.

For the pressure dependence, the following was used:

$$\rho_E \mu_E / \rho_C \mu_C = 0.225 (p/p_C)^{0.992}$$

This fit also has a deviation of about ½%.

Prandtl Number

The dependence of Prandtl number on pressure is neglected, and its variation with enthalpy is a fit of Hansen's data.[8] A precondition for the validity of an effective Prandtl number is that the gas must be in local thermodynamic equilibrium.

Bade Curve-Fits

The density curve-fits from Cohen do not yield good accuracy at low enthalpy levels. Better values of density are obtained using curve-fits suggested by Bade.[16]:

$$\rho/\rho_B = (p/p_B)\,(h/h_B)^{-x}$$

where

$$x = 0.70 + 0.40 \log_{10}(p/p_B) \quad \text{if} \quad 31.9 < h/RT_0 \leq 480$$

$$= 0.94 \quad \text{if} \quad h/RT_0 \leq 31.9$$

The fits have a maximum deviation of 7%.

The viscosity and Prandtl number are then evaluated as in the Cohen curve-fits.

Reference Quantities in Curve-Fits

The following reference quantities were used in the calculations:

$h_C = 2.0108 \times 10^7$ J/kg

$p_C = 1.0$ atm

$\mu_C = 1.716 \times 10^5$ kg/m-s

$\rho_C = 1.2874$ kg/m^3

$\rho_B = 0.1602$ kg/m^3

$h_B = 2.512 \times 10^6$ J/kg

$p_B = 1.0$ atm

Method of Solution

Davis[17] presented an implicit finite-difference method to solve the viscous shock-layer equations for axially symmetric flows. Murray and Lewis[4] extended the method of solution to three-dimensional high-angle-of-attack conditions. The present method of solution is identical to that of Murray and Lewis. Therefore only an overview of the solution procedure is presented here.

The equations are written in the standard parabolic form

$$A_0 \frac{\partial^2 W}{\partial \eta^2} + A_1 \frac{\partial W}{\partial \eta} + A_2 W + A_3 + A_4 \frac{\partial W}{\partial s} + A_5 \frac{\partial W}{\partial \phi} = 0$$

The derivatives are evaluated by the finite-difference expressions used by Frieders and Lewis[18] and substituted into the parabolic equation giving the standard finite-difference form. The difference equation can be solved by the method developed by Richtmyer.

The continuity and normal momentum equations are solved by a similar method, but they are coupled together. Finally, the shock-standoff distance is evaluated by integrating the continuity equation as discussed by Murray and Lewis.[4]

The solution begins on the spherically blunted nose by obtaining an axisymmetric solution in the wind-fixed coordinate system. At a specified location, the axisymmetric solution is rotated into the body-fixed coordinates and used as the initial profile for the three-dimensional solution. The three-dimensional solution begins on the windward plane and marches around the body obtaining a converged solution at each ϕ step. After completing a sweep in ϕ, the procedure then steps downstream in s and begins the next ϕ sweep. At each point the equations are solved in the following order: 1) ϕ-momentum, 2) energy, 3) s-momentum, 4) integration of continuity for n_{sh}, and 5) the coupled continuity and normal momentum equations.

Results and Discussion

The freestream conditions used for the three altitudes are tabulated in Table 1, while the sample cases presented are shown in Table 2. The flow was assumed to be turbulent at 12,192 m and laminar at 24,384 and 48,768 m altitudes. The dimensions of the 7-deg half-angle spherically blunted cone are shown in Fig. 1. The angles of attack considered were 0, 2, 10, and 20 deg. The three wall conditions were a cold wall (300 K), a cool wall (2000 K), and an adiabatic wall.

Test Case Results

A wide range of conditions was solved, but only a few sample results are presented to show typical trends.

There is a significant change in the shock standoff distance for perfect gas and air in chemical equilibrium (Fig. 2). The

Table 1 Freestream conditions

Altitude, h (m)	12,192	24,384	48,768
M_∞	20.6	20.4	18.4
Velocity, U_∞ (m/s)	6096	6096	6096
Pressure, p_∞ (kN/m^2)	18.821	2.801	0.093
Temperature, T_∞ (K)	216.65	220.95	270.65
Density, ρ_∞ (kg/m^3)	3.0268E−1	4.4173E−2	1.1967E−3
Reynolds number (per m)	1.2055E+7	1.7310E+6	3.9776E+4

Table 2 Test cases

Case	α, deg	Altitude, m	T_w, K	T_w/T_∞	Flow
A	0	24,384	300	1.36	Laminar
B	2	12,192	2000	9.16	Turbulent

Table 3 Force and moment data (case A); $\alpha = 0$ deg, altitude = 24,384 m, $T_w = 300$ K, $S/R = 30$

	Actual values			
	PG	TLU	Cohen	Bade
$C_{A_{INV}}$	0.070216	0.076465	0.076465	0.076465
C_{A_P}	0.068310	0.075380	0.075090	0.075570
$C_{A_{SF}}$	0.002510	0.002450	0.002090	0.002180
$C_{A_{TOT}}$	0.070824	0.077835	0.077176	0.077757
Time,[a]	72	233	102	100

	Percent variation based on TLU		
	PG	Cohen	Bade
$C_{A_{INV}}$	8.2	0.0	0.0
C_{A_P}	9.4	0.4	−0.3
$C_{A_{SF}}$	−2.4	14.7	11.0
$C_{A_{TOT}}$	9.0	0.8	0.1
Time,[b] s	33	44	43

[a] IBM 370/3032 with FORTHX compiler (OPT2). [b] Based on TLU = 100.

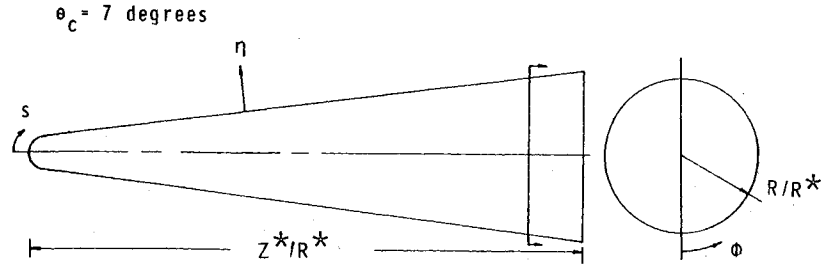

Fig. 1 Nondimensional body geometry and coordinate system.

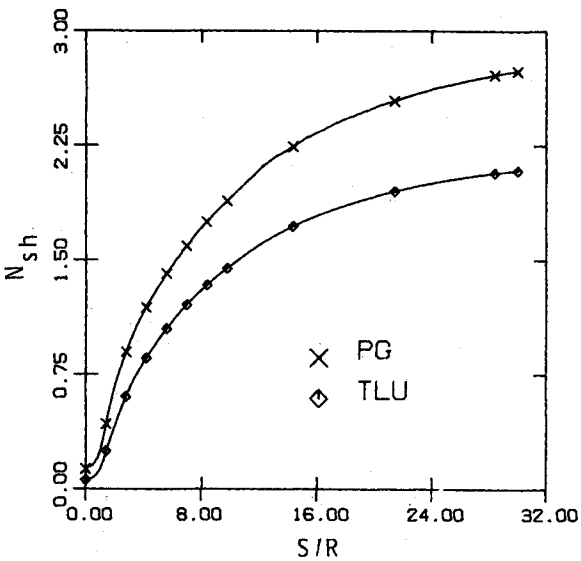

Fig. 2 Streamwise variation of shock-standoff distance (case A, $\alpha = 0$ deg, altitude = 48,768 m, $T_w = 2000$ K).

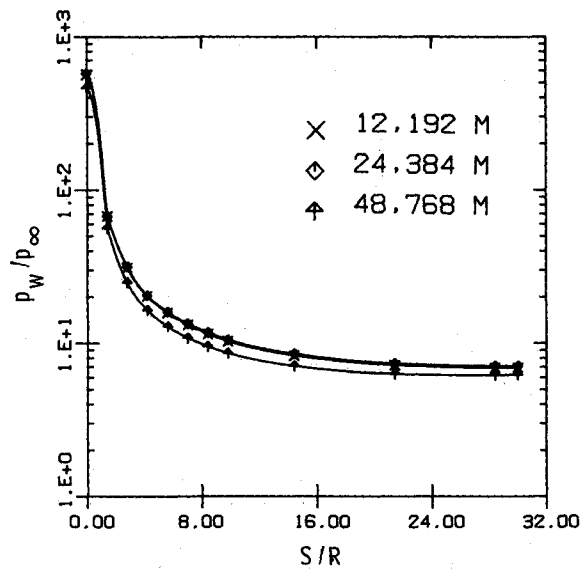

Fig. 3 Streamwise variation of wall pressure (case A, $\alpha = 0$ deg, altitude = 12,192, 24,348, and 48,768 m, $T_w = 300$ K).

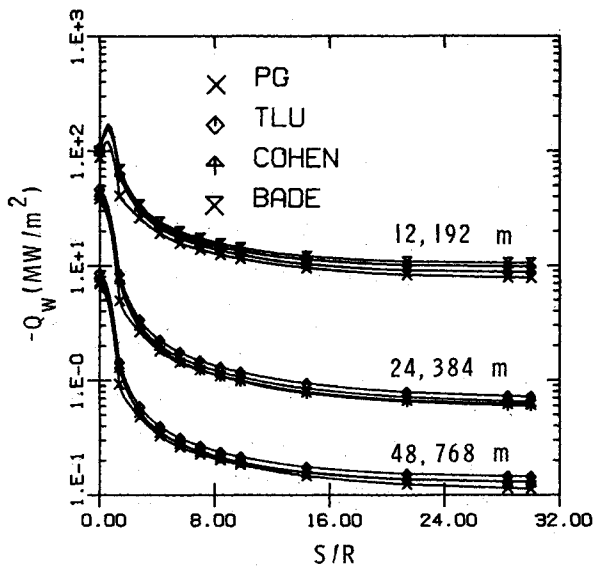

Fig. 4 Streamwise variation of wall heat-transfer rate (case A, $\alpha = 0$ deg, altitude = 12,192, 24,348, and 48,768 m, $T_w = 300$ K).

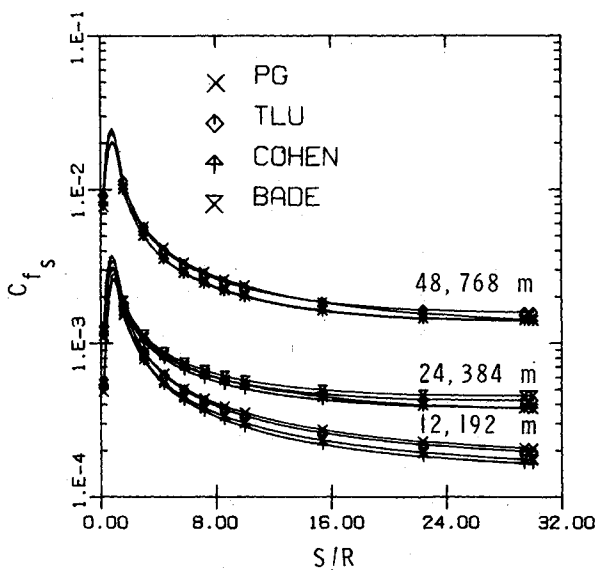

Fig. 5 Streamwise variation of C_{fs} (case A, $\alpha = 0$ deg, altitude = 12,192, 24,348, and 48,768 m, $T_w = 300$ K).

shock-layer thickness is nearly the same for all options of the equilibrium properties.

Case A ($\alpha = 0$ *deg*)

The streamwise variation of wall pressure with altitude show very little differences (Fig. 3) at 12,192 and 24,384 m altitudes, but lower values are predicted for 48,768 m. These values are nearly identical for all the gas models except within the nose region.

The streamwise variation of the wall heat-transfer rate is shown in Fig. 4 for all the cases. In general, the perfect gas and table look-up values are the lowest and highest, respectively, with the Cohen and Bade values lying in between.

The variation of streamwise skin-friction coefficient shows trends similar to those for the wall heat-transfer rate (Fig. 5). For some cases, the Cohen and Bade results do not lie within the band of perfect gas and table look-up results, while these

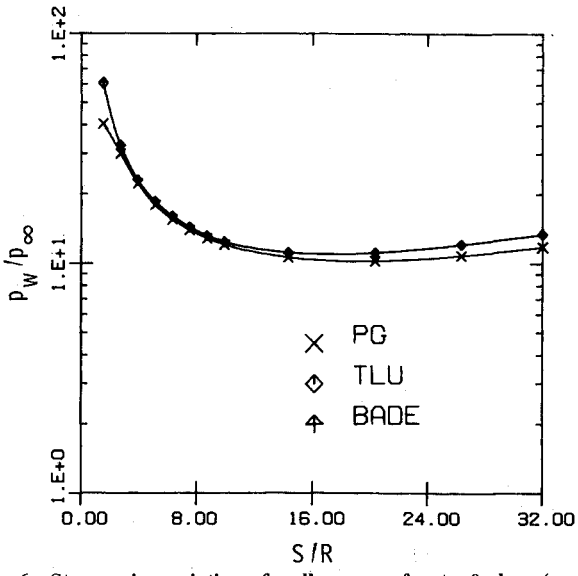

Fig. 6 Streamwise variation of wall pressure for $\phi = 0$ plane (case B, $\alpha = 2$ deg, altitude = 12,192 m, $T_w = 2000$ K).

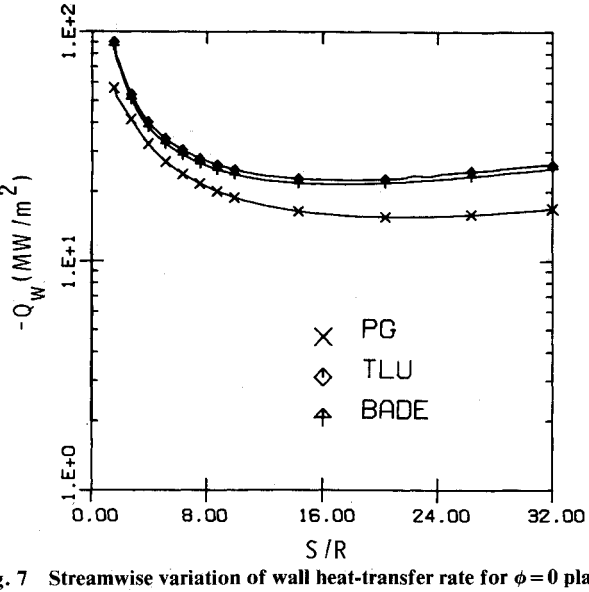

Fig. 7 Streamwise variation of wall heat-transfer rate for $\phi = 0$ plane (case B, $\alpha = 2$ deg, altitude = 12,192 m, $T_w = 2000$ K).

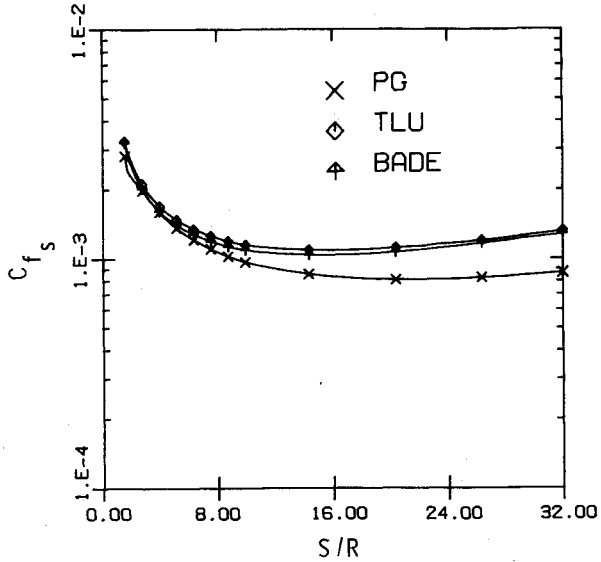

Fig. 8 Streamwise variation of C_{f_s} for $\phi = 0$ plane (case B, $\alpha = 2$ deg, altitude = 12,192 m, $T_w = 2000$ K).

Table 4 Force and moment data (case B); $\alpha = 2$ deg, altitude = 12,192 m, $T_w = 2000$ K, $S/R = 32$

	Actual values			Percent variation based on TLU	
	PG	TLU	Bade	PG	Bade
$C_{A_{INV}}$	0.063311	0.065495	0.065495	3.3	0.0
$C_{N_{INV}}$	0.034556	0.039216	0.039216	11.9	0.0
$C_{A_{TOT}}$	0.071163	0.078564	0.078414	9.4	0.2
C_N	0.032386	0.038607	0.038653	16.1	−0.1
C_M	−0.021207	−0.025800	−0.025856	17.8	−0.2
Z_{cp}/L	0.654814	0.668288	0.668924	2.0	−0.1
$C_{A_{SF}}$	0.00595	0.00744	0.00718	20.0	4.6
C_{A_P}	0.06521	0.07112	0.07132	8.3	−0.3
Time	1778[a]	5203[a]	2384[a]	34[b]	46[b]

[a] Seconds IBM 370/3032 with FORTHX compiler (OPT2). [b] Based on TLU = 100.

Table 5 Comparison of heat-transfer coefficients[a] in percent based on TLU; $\alpha = 0$ deg, altitude = 12,192 m, $T_w = 2000$ K, $S/R = 32$, laminar flow.

	PG	Cohen	Bade
Q_w	80.8	79.4	88.8
$\partial h/\partial \eta$	93.3	99.0	94.8
n_{sh}	113.6	124.4	98.0
ρ	95.8	88.9	98.9
μ	90.4	94.1	86.7
Pr	91.8	94.1	94.1

[a] $Q_w \propto -(\mu/n_{sh}Pr)(\partial h/\partial \eta)$.

differences are quite small for the Cohen and Bade results (Table 3).

Case B ($\alpha = 2$ deg)

The variation of the wall pressure for the windward plane is shown in Fig. 6. The pressures from the table look-up and Bade options are nearly identical. On the spherical nose, the differences between perfect gas and table look-up are substantial, and after tending together for some distance, they again tend to diverge.

The wall heat-transfer rate for the windward plane from the perfect gas prediction is about 10% less than the table look-up results (Fig. 7) and diverges downstream. The difference between the table look-up and Bade data is fairly small (within 2%).

The streamwise skin-friction coefficient results are similar to the wall heat-transfer rate (Fig. 8) data.

The transverse variation of wall pressure (Fig. 9), wall heat-transfer rate (Fig. 10), and streamwise (Fig. 11) and transverse (Fig. 12) skin-friction coefficients show similar trends.

The variations in the force and moment data for one case are shown in Table 4. The inviscid axial and normal force coefficients for perfect gas conditions are 4 and 12% less than the table look-up results, and while the viscous axial and normal force coefficients are 9 and 16% less. The variation of the center of pressure is about 2%. The differences between the table look-up and Bade results are much smaller and quite acceptable.

The present differences between perfect gas and equilibrium air results were the highest for the $\alpha = 2$ deg case, being lower for both the $\alpha = 10$ and 20 deg cases.

Table 5 shows the values of various quantities that are used to evaluate the heat-transfer rate for all the gas models used. Here the values are compared to a TLU value of 100.

For perfect gas the 19% reduction in heat-transfer rate is caused by a 7% reduction in $\partial h/\partial \eta$ and a 14% increase in n_{sh} caused by a 4% reduction in density.

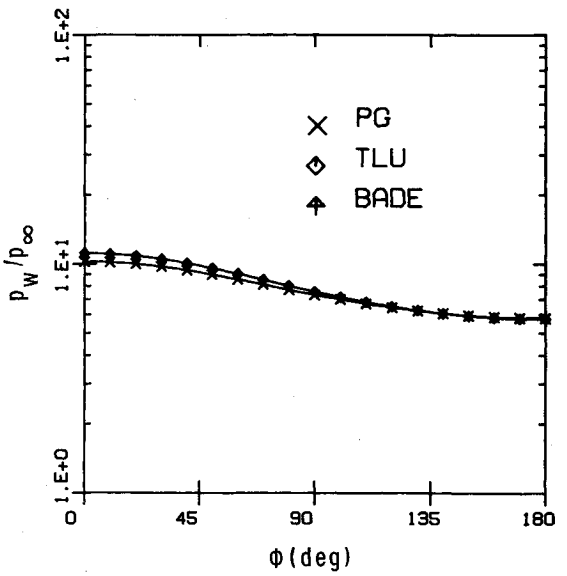

Fig. 9 Transverse variation of wall pressure at $S/R=20$ (case B, $\alpha=2$ deg, altitude = 12,192 m, $T_w=2000$ K).

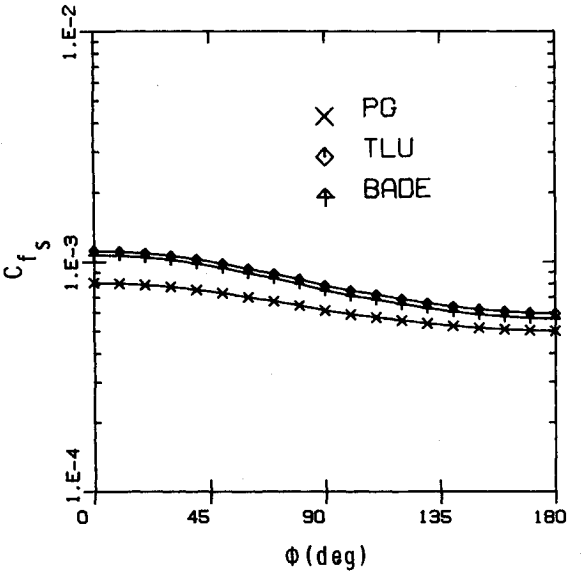

Fig. 11 Transverse variation of C_{f_s} at $S/R=20$ (case B, $\alpha=2$ deg, altitude = 12,192 m, $T_w=2000$ K).

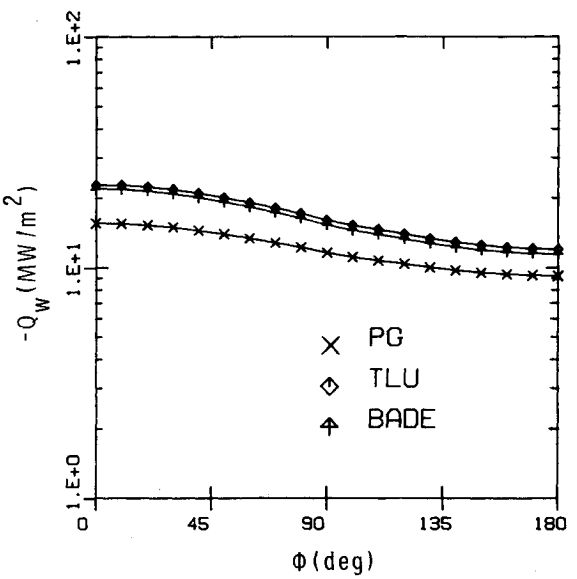

Fig. 10 Transverse variation of wall heat-transfer rate at $S/R=20$ (case B, $\alpha=2$ deg, altitude = 12,192 m, $T_w=2000$ K).

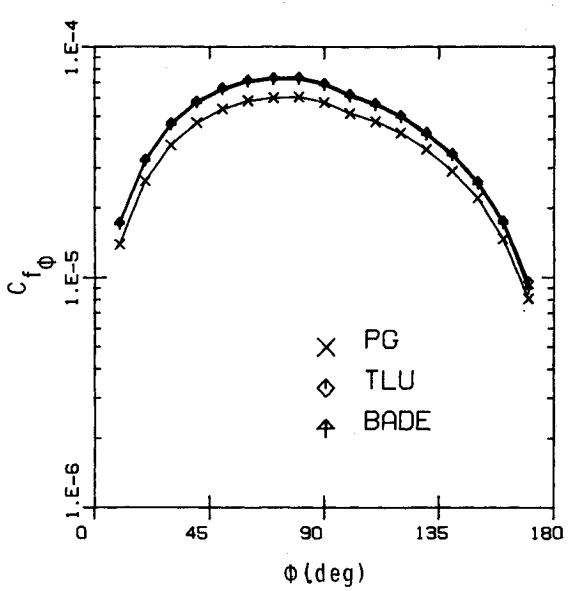

Fig. 12 Transverse variation of C_{f_ϕ} at $S/R=20$ (case B, $\alpha=2$ deg, altitude = 12,192 m, $T_w=2000$ K).

For the curve-fit equilibrium air models, the contributions are more complex. The 11% reduction in heat-transfer rate for Bade curve-fits is mainly due to the 13, 5, and 6% reductions in viscosity, $\partial h/\partial\eta$, and Prandtl number, respectively. For Cohen curve-fits, the 20% reduction in heat-transfer rate is caused mainly by the large reduction in density which results in a 24% increase in the shock-standoff distance.

Computing Times Required

Computing times given in the tables are with the table look-up time as a reference of 100. Due to the absence of some input/output for the perfect gas model, the time for this condition is slightly lower than the Cohen and Bade options. If one omits the extra printout, the curve-fits of equilibrium properties and perfect gas computing times are very comparable and result in a 60% reduction in the computing time required for the table look-up model.

For low values of wall temperature, since all the equilibrium models essentially use Sutherland's viscosity and the density from the table look-up and Bade options is in good agreement, the differences in the wall heat-transfer rate are due to the differences in the Prandtl number and the shock-standoff distance.

Conclusions

In general, wall heat-transfer rate differences between the perfect gas and table look-up results are about 10%, while the axial force coefficients differ by 5 to 15%. Large pressure differences in the nose region (which constitutes a significant percentage of the frontal area) cause the large differences in axial force.

Curve-fits can be effectively used to model the thermodynamic and transport properties of air in chemical equilibrium, producing reasonably good force and moment coefficient predictions with computing times that are comparable to the perfect gas model. The differences in wall heat-transfer rate for equilibrium flow are probably caused by the differences in Prandtl number and the shock-standoff distance.

Since there are considerable differences between the perfect gas and equilibrium air results, the viscous shock-layer method just developed should be used to predict viscous flows in chemical equilibrium, such as for ballistic vehicle re-entry conditions, with good accuracy and within reasonable computing times.

References

[1]Miner, E.W., Anderson, E.C., and Lewis, C.H., "A Computer Program for Two Dimensional and Axisymmetric Nonreacting Perfect Gas and Equilibrium Chemically Reacting Laminar Transitional and/or Turbulent Boundary Layer Flows," Virginia Polytechnic Institute, Blacksburg, Va., VPI-E-71-8, May 1971.

[2]Cohen, N.B., "Correlation Formulas and Tables of Density and Some Thermodynamic Properties of Equilibrium Dissociating Air for Use in Solutions of the Boundary Layer Equations," NASA TN D-194, Feb. 1960.

[3]Lubard, S.C. and Helliwell, W.S., "Calculation of Flow in a Cone at High Angle of Attack," *AIAA Journal,* Vol. 12, July 1974, pp. 965-974.

[4]Murray, A.L. and Lewis, C.H., "Hypersonic Three-Dimensional Viscous Shock-Layer Flow over Blunt Bodies," *AIAA Journal,* Vol. 16, Dec. 1978, pp. 1279-1286.

[5]Szema, K.Y. and Lewis, C.H., "Three-Dimensional Hypersonic Laminar, Transitional and/or Turbulent Shock-Layer Flows," AIAA Paper 80-1457, July 1980.

[6]Cebeci, T., "Behavior of Turbulent Flows near a Porous Wall with Pressure Gradient," *AIAA Journal,* Vol. 8, Dec. 1970, pp. 2152-2156.

[7]Dhawan, S. and Narasimha, R., "Some Properties of Boundary Layer Flow During the Transition from Laminar to Turbulent Motion," *Journal of Fluid Mechanics,* Vol. 3, Part 4, Jan. 1958, pp. 418-436.

[8]Hansen, C.F., "Approximations for the Thermodynamic and Transport Properties of High Temperature Air," NASA TR R-50, 1959.

[9]Cebeci, T. and Smith, A.M.O., *Analysis of Turbulent Boundary Layers,* Academic Press, New York, 1974.

[10]Anderson, E.C., Moss, J.N., and Sutton, K., "Turbulent Viscous Shock-Layer Solutions with Strong Vorticity Interaction," AIAA Paper 76-120, Jan. 1976.

[11]Klebanoff, P.S., "Characteristics of Turbulence in a Boundary Layer with Zero Pressure Gradient," NACA Report 1247, 1955.

[12]Clauser, F.H., "The Turbulent Boundary Layer," *Advances in Applied Mechanics,* edited by H.L. Dryder and Th. von Kármán, Academic Press, New York, 1956, pp. 1-15.

[13]White, F.M., *Viscous Fluid Flow,* McGraw-Hill Book Company, New York, 1974.

[14]Lordi, J.A., Mates, R.E., and Moselle, J.R., "A Computer Program for the Numerical Solution of Nonequilibrium Expansions of Reacting Gas Mixtures," Calspan Corp., Buffalo, N.Y., CAL RPT No. AD-K89-A-6, 1965.

[15]Moeckel, W.E. and Weston, K.C., "Composition and Thermodynamic Properties of Air in Chemical Equilibrium," NASA TN 4265, 1958.

[16]Bade, W.L., "Simple Analytical Approximation to the Equation of State of Dissociating Air," *ARS Journal,* Vol. 29, April 1959, pp. 298-299..

[17]Davis, R.T., "Numerical Solution of the Hypersonic Viscous Shock Layer Equations," *AIAA Journal,* Vol. 8, May 1970, pp. 843-851.

[18]Frieders, M.C. and Lewis, C.H., "Effects of Mass Transfer into Laminar and Turbulent Boundary Layers over Cones at Angle of Attack," Virginia Polytechnic Institute, Blacksburg, Va., VPI-AERO-031, March 1975.